Supplementary Information

Nanoscale control over single vortex motion in an unconventional superconductor

*Sang Yong Song, Chengyun Hua, Gábor B. Halász, Wonhee Ko, Jiaqiang Yan, Benjamin J. Lawrie, Petro Maksymovych**

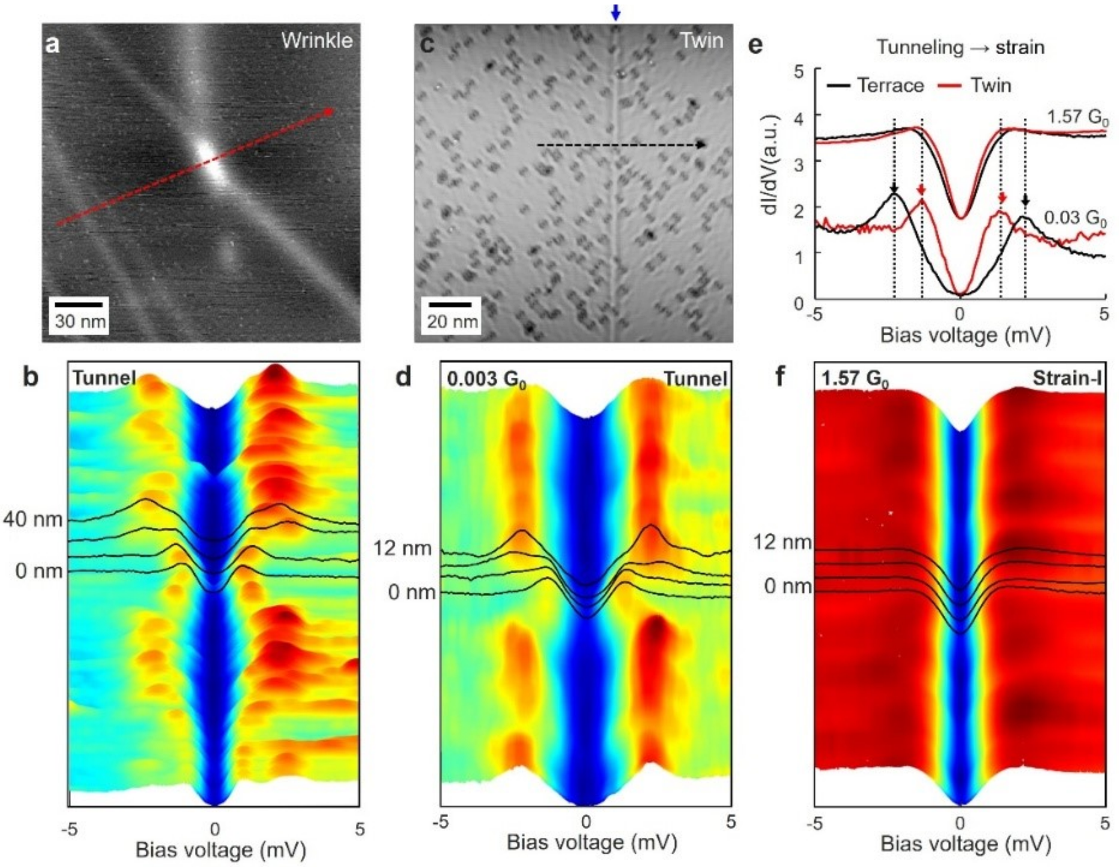

Fig. S1 Reduction of superconducting gaps near a wrinkle, a twin boundary, and at strain induced area. (a) Topographic image of the wrinkle on FeSe. (b) The spatial variation of superconducting gap across the wrinkle (red dashed line in (a)). (c) Topographic image of the twin boundary on FeSe (blue arrow). (d) Spatial variation of superconducting gap across the twin boundary (black dashed line in (c)) in the tunneling regime. (e) dI/dV spectra obtained at low conductance and high conductance on the terrace (black curves) and the twin boundary (red curves). (f) Spatial variation of superconducting gap across the twin boundary (black dashed line in (c)) in the strain-I regime (1.57 G_0).

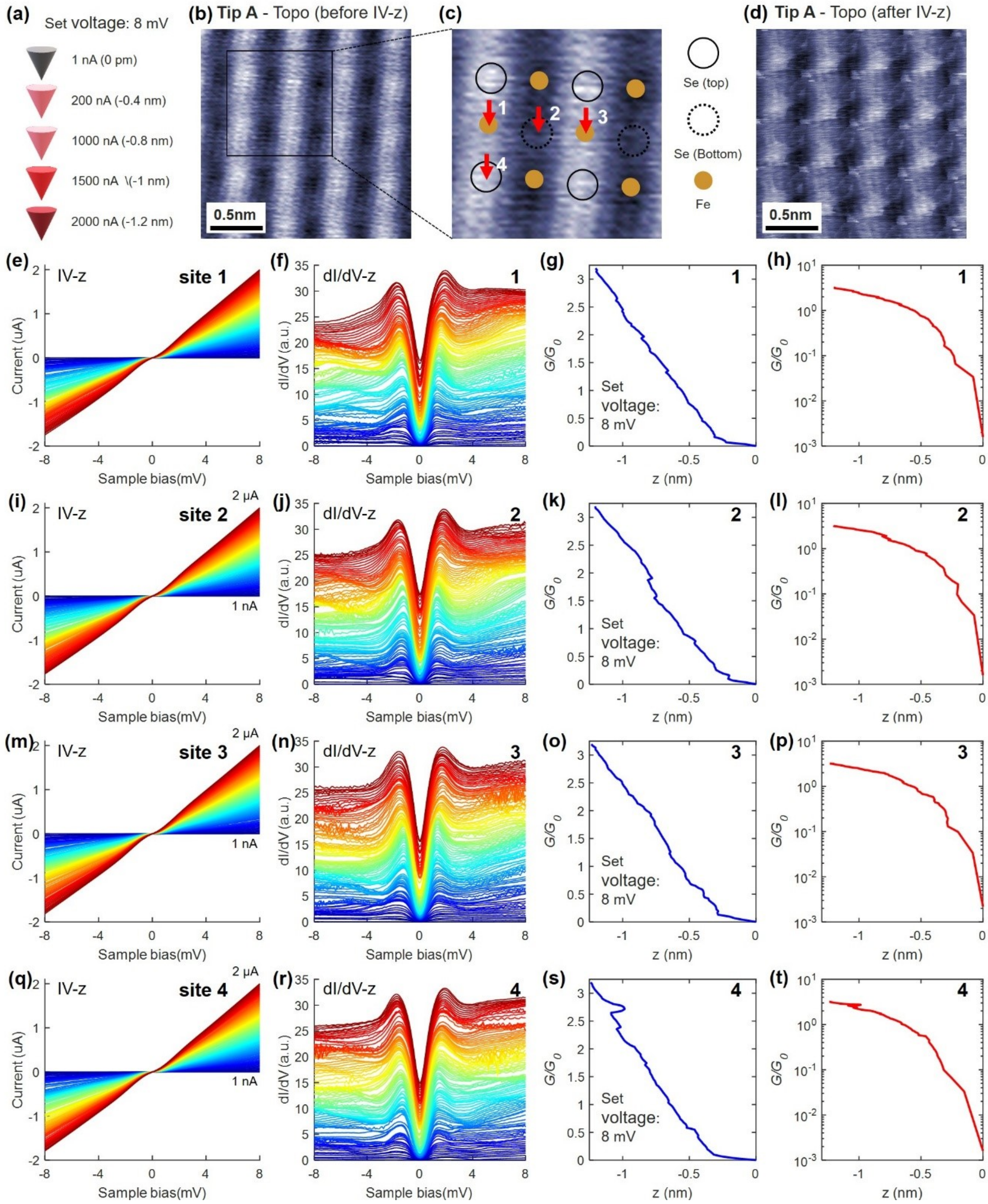

Fig. S2 (a) Schematic of the approach protocol from the initial setpoint (1 nA, z = 0 pm) to higher setpoint currents up to 2000 nA (z ≈ −1.2 nm). (b,c) Atomic-resolution topography acquired before the IV–z sequence, with the measurement sites (1–4) marked; circles indicate the Se(top)/Se(bottom) sublattices and Fe sites. (d) Topography acquired after the IV–z sequence, showing slight change in the morphology. (e–h) Representative results at site 1: I IV–z curves, (f) stacked dI/dV spectra as a function of z, and the corresponding conductance G/G_0 versus z plotted on (g) linear and (h) logarithmic scales. (i–l), (m–p), and (q–t) Same as (e–h) for sites 2–4, respectively. Color encodes the tip displacement (z) during the approach.

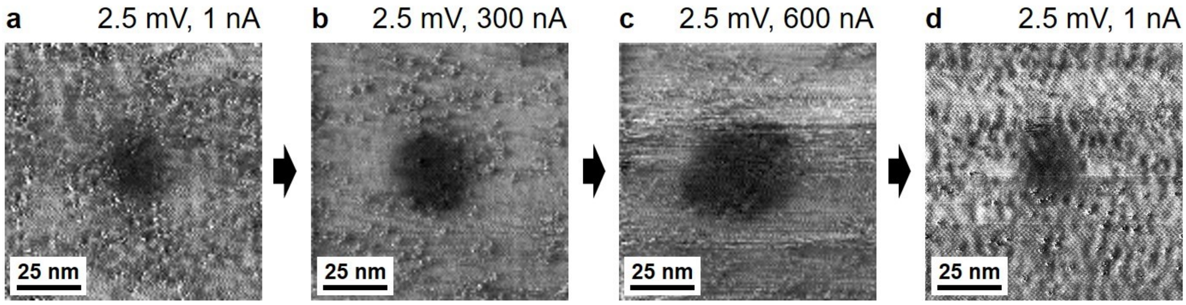

Fig. S3 Single energy conductance maps measured by sequentially changing the set point for one vortex. These conductance maps indicate that the strain-induced modification is reversible.

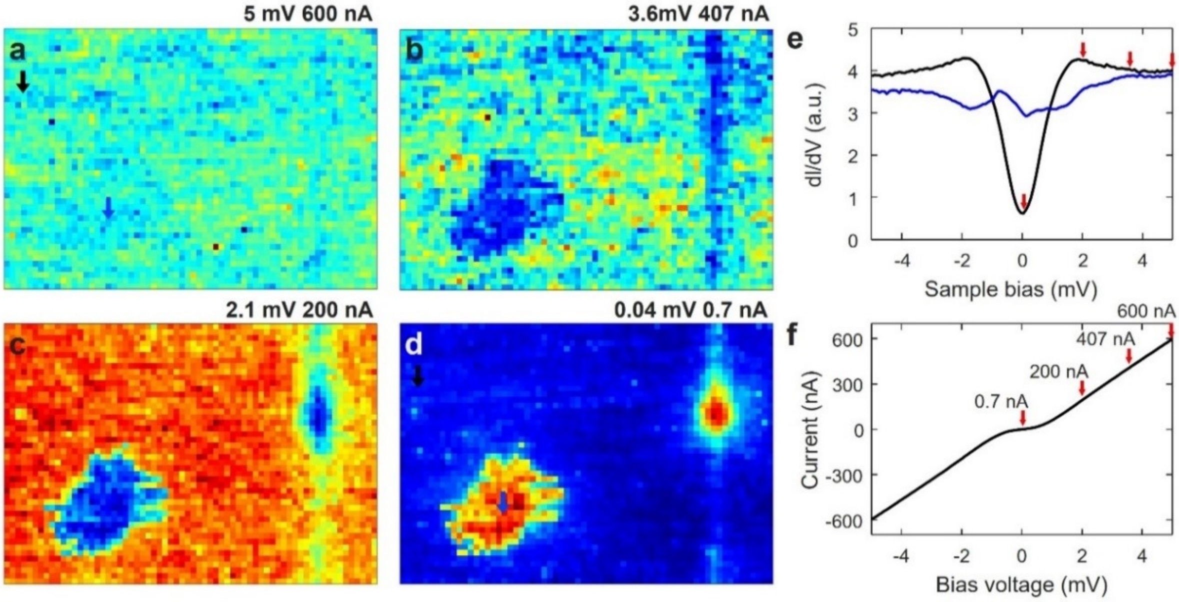

Fig. S4 The size of the expanded vortex at different biases. This data set (main text in Fig. 4d, f, and h) consists of dI/dV spectra at every point (66 x 48 points), with setting conductance at 1.57 G_0. During each dI/dV measurement, the current feedback loop is closed, and the tip position is fixed at the setting point (set conductance value). (a-d) Differential conductance maps at 5 mV, 3.6 mV, 2.1 mV, and 0.04 mV extracted from the dI/dV mapping. (e) The superconducting gaps on the terrace (black) and on the vortex core (blue). The red arrows indicate the positions of voltages at 0.04 mV, 2.1 mV, 3.6 mV, and 5mV. (f) The I-V curve during measuring the dI/dV curve in (e). The red arrows indicate the bias values and corresponding currents.

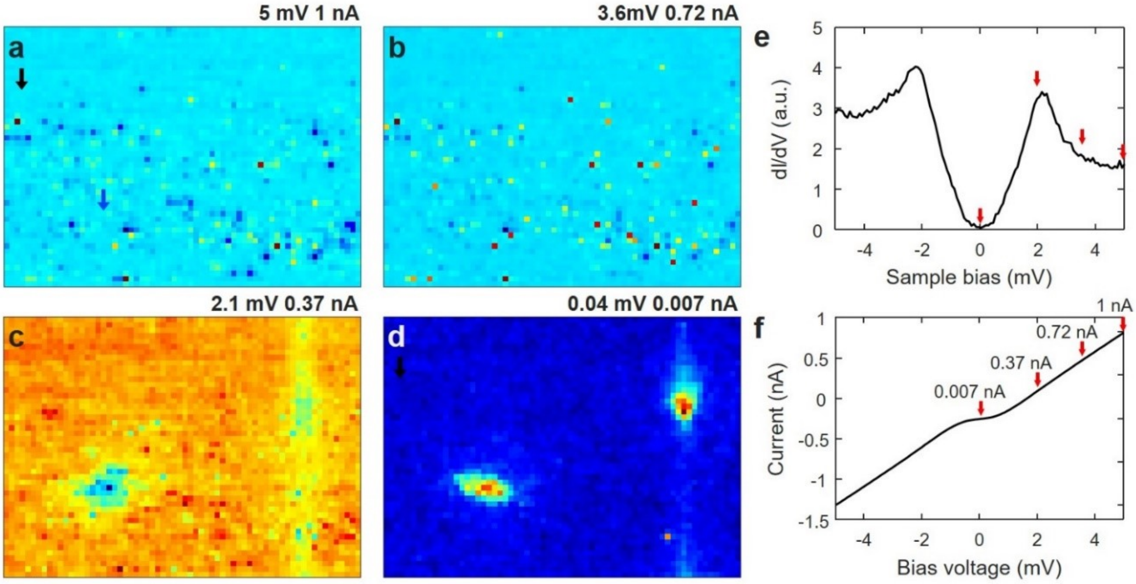

Fig. S5 The size of the normal vortex at different biases. This data set (main text in Fig. 4c, e, and g) consists of dI/dV spectra at every point (66 x 48 points), with setting conductance at 0.003 G_0 (tunneling). During each dI/dV measurement, the current feedback loop is closed, and the tip position is fixed at the setting point (set conductance value). (a-d) Differential conductance maps at 5 mV, 3.6 mV, 2.1 mV, and 0.04 mV extracted from the dI/dV mapping. (e) The superconducting gaps on the terrace. The red arrows indicate the positions of voltages at 0.04 mV, 2.1 mV, 3.6 mV, and 5mV. f) The I-V curve during measuring the dI/dV curve in (e). The red arrows indicate the bias values and corresponding currents.

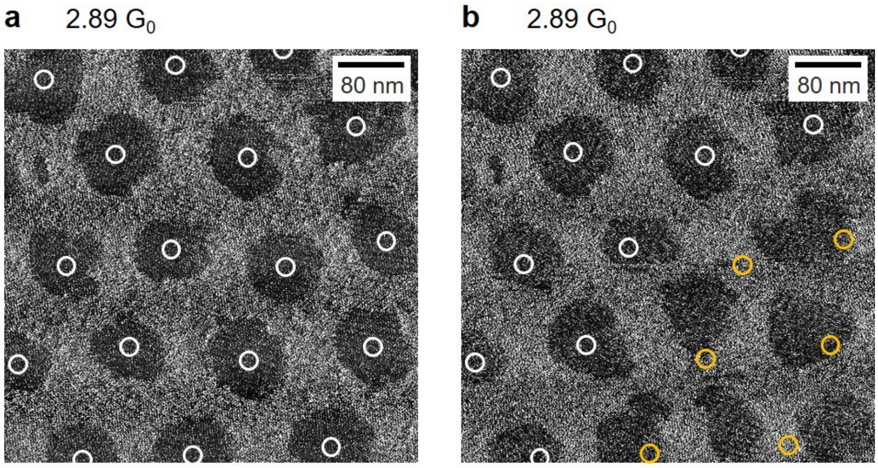

Fig. S6 Changing the partial array of vortex lattice during the high current mapping. (a) Conductance map of expanded vortices at 2.89 G_0 (-2.5 mV, 560 nA). (b) Conductance map of locally changed vortex array (yellow dots) at 2.89 G_0 (-2.5 mV, 580nA).

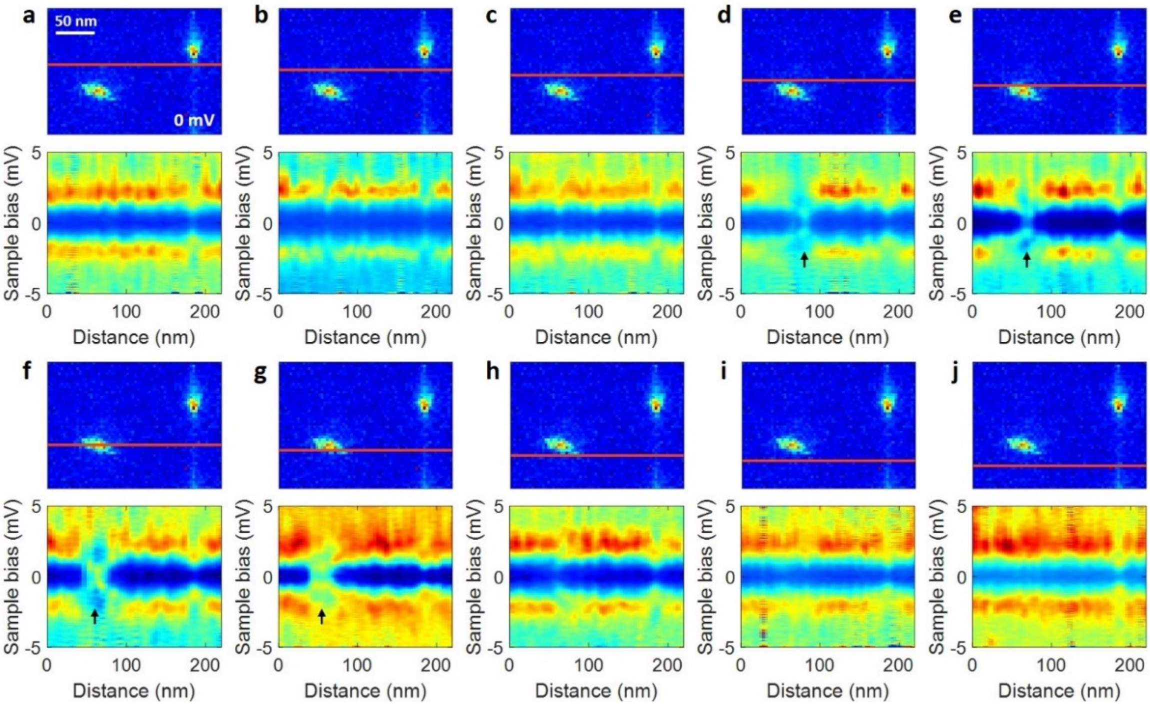

Fig. S7 (a-j) Zero bias conductance maps that contain a vortex on the terrace and a vortex on the twin boundary in tunneling regime (0.003 G_0), and the spatial variations of superconducting gaps across the vortex on the terrace in tunneling regime (0.003 G_0).

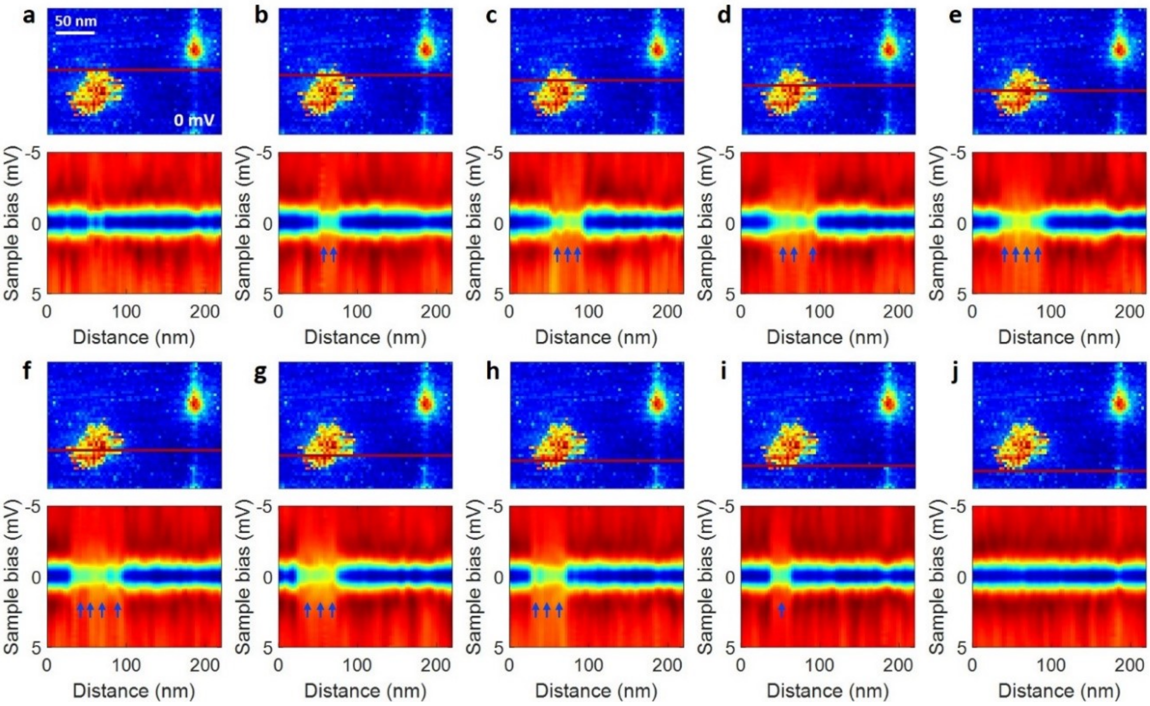

Fig. S8 (a-j) Zero bias conductance maps that contain a vortex on the terrace and a vortex on the twin boundary at 1.57 G_0 ($V_{set} = 5$ mV, $I_{set} = 600$ nA), and the spatial variations of superconducting gaps across the vortex on the terrace at 1.57 G_0.

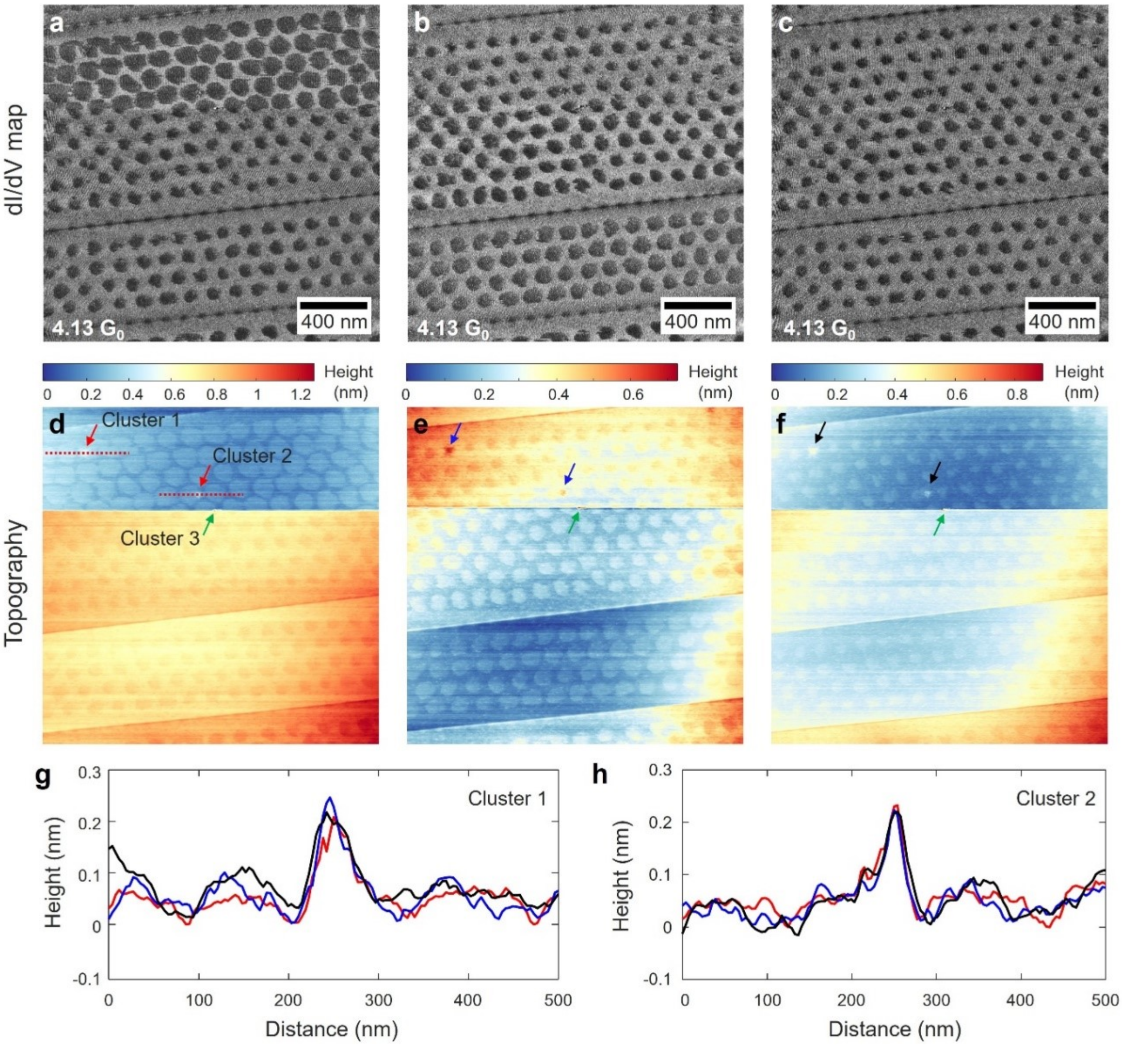

Fig. S9 Sensitivity of vortex displacement to changing STM tip structure. (a-c) Differential conductance maps of expanded vortices as tip changes at 2.5 mV, 800 nA (4.13 G_0). (d-f) Topographic images of the expanded vortices, twin boundaries, and clusters as tip changes (setpoint: V_{bias} = 2.5 mV, I = 800 nA). There are three clusters (red and green arrows in (d). The cluster 3 (green arrow in (d)) continuously changes the tip apex during the differential conductance mapping. (g, h) Topographic line profiles across the cluster 1 and cluster 2 for the different tip apexes in (d), (e), and (f).

Supplementary Note 1 – Evaluation of voltage division effects in the contact regime

In the contact and high-conductance regime, apparent shifts of spectral features could, in principle, arise from voltage division due to external circuitry rather than intrinsic changes in the sample. Here we quantitatively evaluate the magnitude of such effects in our experimental setup. In our STM system, the sample bias from the STM controller is applied through a Unisoku bias attenuator (UBDF-200) operated in the 1/100 attenuation mode, which has an input impedance of 10 kΩ. This attenuator can be regarded as a passive voltage divider. In this configuration, the effective Thevenin output resistance of the attenuator is approximately $R_{out} \sim R_{top} \,||\, R_{bottom} \approx 100\ \Omega$ (e.g., $R_{top} \approx 9.9$ kΩ, $R_{bottom} \approx 100\ \Omega$). The actual tip–sample voltage V_{ts} is therefore given by

$$V_{ts} = V_{set}\frac{R_j}{R_j + R_{out}}$$

Indicating a reduction of only about 2.4% due to voltage dvision. Such a small reduction would lead to apparent shifts of spectral features at energies of ±1 - ±1.5 mV by only

$$\Delta V \approx V_0\left(\frac{1}{0.976} - 1\right) \approx 0.976$$

Which is more than an order of magnitude smaller than the energy shifts observed in Fig. 2. We therefore conclude that voltage division effects arising from the external bias circuitry are quantitatively negligible under the experimental conditions used in this work.

Supplementary Note S2 – Analytical description of expanded vortex core

In a reference [S1], the formula for the force per unit length between two vortex lines separated by distance r is given by

$$f = \frac{\Phi_0^2}{2\pi\mu_0\lambda^3}K_1\left(\frac{r}{\lambda}\right)$$

Here, Φ_0 is the quantized magnetic flux (2.07 x 10^{-15} Wb), μ_0 is the vacuum permeability (4π x 10^{-7} H/m), and λ is the London penetration depth (~400 nm), K_1 is the modified Bessel function of the second kind. If we assume that only a short section of the vortex line with length on the order of λ is moved, the force becomes $\Phi_0^2/2\pi\mu_0\lambda^2 \cdot K_1(1)$, which is about 2 pN.

Supplementary Note S3 – Analytical description of expanded vortex core

For the size of inclusion comparable to the coherence length ($a_x \sim \xi$), the vortex binding energy to an anisotropic inclusion is given by$^{2-4}$

$$U_p \approx \varepsilon_0 a_z \ln\left(1 + \frac{a_x^2}{\xi_{ab}^2}\right) \tag{1}$$

Where $\varepsilon_0 = \Phi_0^2/4\pi\mu_0\lambda^2$ is the typical vortex energy scale, λ is the London penetration depth (~ 400 nm), the a_x is the inclusion size of the x-axis, a_z is the inclusion size of the z-axis, and ξ_{ab} is the coherence length for the ab-plane. We can obtain the pinning force f_p by dividing the vortex pinning energy by the inclusion size a_x.

$$f_p \approx \varepsilon_0 \frac{a_z}{a_x} \ln\left(1 + \frac{a_x^2}{\xi_{ab}^2}\right) \tag{2}$$

Furthermore, Willa, R. et al.[4] adapted dimensionless functions $G_i(\gamma a_z/a_x)$ to pinning force to describe the dependence of size and anisotropy for the large defects ($a_x \gg \xi$). The dimensionless functions contain the defect's aspect ratio (a_z/a_x) and the anisotropy parameter γ ($\gamma = \xi_{ab}/\xi_c$) of the superconductor. In a similar way, we can adapt the dimensionless functions $G_i(\gamma a_z/a_x)$ to equation (2) which describes a relatively small defect ($a_x \sim \xi$).

$$f_p(a_x, a_z, \gamma) \approx G_1\left(\frac{\gamma a_z}{a_x}\right) \frac{\varepsilon_0}{\gamma} \ln\left(1 + G_2\left(\frac{\gamma a_z}{a_x}\right) \frac{a_x^2}{\xi_{ab}^2}\right) \tag{3}$$

The deformation of the vortex line is determined by the balance between the elasticity of the vortex line and the pinning force,[5,6]

$$f_p(x) = \bar{C}u \tag{4}$$

Where $\bar{C}$ is the effective spring constant and relates to the elastic Green's function.[7] For a small pinning center, $\bar{C} \approx 3\sqrt{\varepsilon_1 \varepsilon_0}/a_\Delta$ is constant.[4,5] Where, $\varepsilon_1 \approx \varepsilon_0/\gamma^2$ is the vortex line tension, and a_Δ is the vortex lattice constant (~ 140 nm at 0.13 T on FeSe). From these results, we fitted the dependence of deformations of vortex lines on the conductance values obtained from various tips (red, black, and blue circles in Fig. 5c in main text) with the form of $A \cdot \ln(1 + B \cdot x^2)$ (red, black, and blue dotted lines in Fig. 5c in main text and Fig. S10). We confirmed that the strength of deformation of the vortex line is determined by the defect's aspect ratio (a_z/a_x).

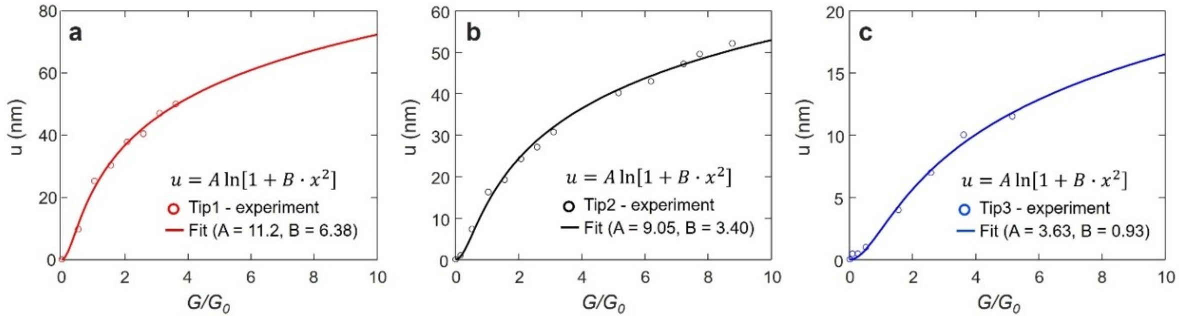

Fig. S10 (a-c) Dependence of vortex line deformation, u, on conductance values obtained from tip1 (red), tip2 (black), and tip3 (blue), with line fitting based on $A\ln[1 + B \cdot x^2]$.

References

(S1) M. Tinkham, Introduction to Superconductivity, 2nd ed., Dover Publications, New York, 2004, p. 154.
(S2) C. J. van der Beek, M. Konczykowski, A. Abal'oshev, I. Abal'osheva, P. Gierlowski, S. J. Lewandowski, M. V. Indenbom and S. Barbanera, *Phys. Rev. B,* 2002, **66**, 024523.
(S3) A. E. Koshelev and A. B. Kolton, *Phys. Rev. B,* 2011, **84**, 104528.
(S4) C. J. van der Beek, M. Konczykowski and R. Prozorov, *Supercond. Sci. Technol.,* 2012, **25**, 084010.
(S5) R. Willa, A. E. Koshelev, I. A. Sadovskyy and A. Glatz, *Phys. Rev. B,* 2018, **98**, 054517.
(S6) R. Willa, A. E. Koshelev, I. A. Sadovskyy and A. Glatz, *Supercond. Sci. Technol.,* 2018, **31**, 014001
(S7) G. Blatter, V. B. Geshkenbein and J. A. G. Koopmann, *Phys. Rev. Lett.,* 2004, **92**, 067009.